

Enhancing Layer Attention Efficiency through Pruning Redundant Retrievals

Hanze Li^{a,†} and Xiande Huang^{*}

^aUniversity of Electronic Science and Technology of China

^{*}De Artificial Intelligence Lab

Abstract. Growing evidence highlights the impact of layer attention mechanisms in deep neural networks, which enhance inter-layer interactions and representational ability. However, existing layer attention methods suffer from redundancy, as adjacent layers often learn highly similar attention weights. This redundancy leads to multiple layers retrieving nearly identical features, diminishing the model’s representational capacity and increasing training time. To address this issue, we propose an Efficient Layer Attention (ELA) architecture composing two key components: first, we quantify redundancy by leveraging Kullback-Leibler (KL) divergence between adjacent layers; second, we introduce an Enhanced Beta Quantile Mapping (EBQM) algorithm to accurately detect and skip redundant retrieving, ensuring model stability while boosting efficiency. Experimental results demonstrate that ELA not only enhances overall performance but also reduces training time by 30%, yielding improvements in tasks such as image classification and object detection.

1 Introduction

Numerous studies have demonstrated that enhancing inter-layer interactions in deep convolutional neural networks (DCNNs) can substantially improve performance across various tasks. For instance, ResNet [10] introduced skip connections to facilitate gradient flow, effectively mitigating the issue of performance degradation in very deep networks. Building upon this idea, DenseNet [15] further strengthened layer interactions by reusing information from all previous layers. In addition to these innovations, attention mechanisms have also played a crucial role in boosting model performance. Channel attention mechanisms [13, 34, 27, 23], refine feature selection by prioritizing the most informative channels, enabling the network to focus on the salient feature maps. Complementarily, spatial attention mechanisms [37, 35, 17, 36] improve the network’s ability to model spatial hierarchies by directing attention to the most relevant spatial regions, thereby refining the learned representations.

Recently, enhancing inter-layer interactions through layer attention mechanisms has emerged as an effective strategy for improving model’s representational ability. DIANet [16] introduced an improved LSTM block along the depth of the network to facilitate interactions between layers. Similarly, RLANet [41] employs a lightweight recurrent aggregation module to effectively reuse information from previous layers. BViT [18] further aggregates the outputs of each Transformer layer in the ViT [7] architecture through

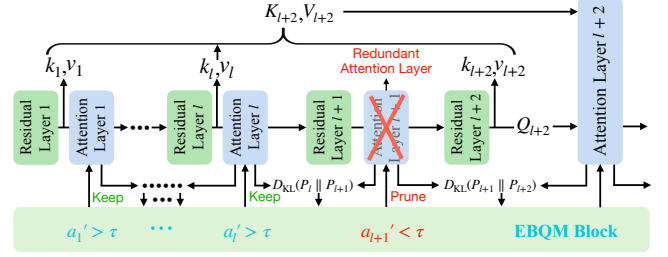


Figure 1: Framework of our ELA: First, the KL divergences of attention scores learned by adjacent layers are computed. These divergences are then fed into the EBQM block and mapped into a target distribution, yielding normalized importance scores $a'_1, \dots, a'_l, a'_{l+1}$. Finally, attention layers with $a'_i < \tau$ are pruned.

attention mechanism, significantly boosting overall performance. MUDD [38] enhances layer interaction through dynamic connection weights, which depends on each sequence position in a Transformer block. To further enhance cross-layer interaction, MRLA [8] introduced layer attention that leverages a multi-head attention across layers to align features from current layer with those from all preceding layers. Building upon this, Wang et al. argued that MRLA operates in a static manner, which limits its efficiency. To address this, they proposed Dynamic Layer Attention (DLA) [33], which restores the dynamic context representation for more efficient layer attention.

However, we have identified a significant drawback in existing layer attention mechanisms: the redundant retrieval for previous feature across layers. As shown in Figure 2a, the attention weights learned by three consecutive layers (the 4th, 5th, and 6th) are nearly identical, all heavily focusing on the 2nd layer. This consistent retrieval pattern is not merely a coincidence—it indicates a systemic redundancy in the attention mechanism. When multiple layers repeatedly attend to the same previous features, the model wastes computation and fails to fully exploit the expressive potential of deeper layers. This issue becomes particularly evident in practice. As shown in Figure 2b, when the network depth exceeds 56 layers, the performance of MRLA-B declines as the depth increases, and with ResNet-110 as the backbone, its accuracy even drops below that of the original ResNet-110 baseline. Although MRLA-L maintains performance gains as the network deepens, the improvement slows down, primarily due to the reduced training efficiency caused by redundant attention patterns.

Based on these observations, we propose a key research question: **Is it necessary to relearn similar attention patterns in each layer?** Instead of repeatedly retrieving the same earlier features, later lay-

^{*} Corresponding Author. Email: xdhuang@dail.email

[†] Work performed while at De Artificial Intelligence Lab

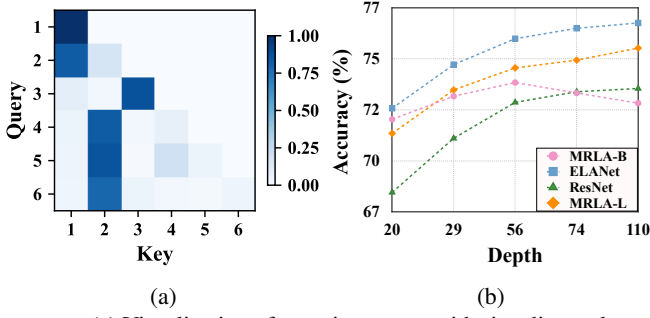


Figure 2: (a) Visualization of attention scores with six adjacent layers in layer attention for ResNet-56 (stage 2). (b) Top1-accuracy comparison of MRLA-B, MRLA-L, ELANet (with ResNet as the backbone) and ResNet at varying depths.

ers—such as the 5th and 6th—can skip the layer attention operation entirely when redundancy is detected, since the relevant information has already been retrieved by the preceding layer. This not only reduces computational overhead, but also alleviates the issue of over-representing certain features, leading to more efficient and balanced information flow across the network.

To address this issue, we propose an Efficient Layer Attention (ELA) architecture consisting of two key components: ① a KL divergence-based strategy to quantify attention redundancy, and ② an Enhanced Beta Quantile Mapping (EBQM) algorithm to guide the pruning of redundant retrievals. Specifically, we treat attention weights in each layer as probability distributions and compute the KL divergence between successive layers. A low KL divergence indicates that the attention behavior of the current layer is highly similar to that of the previous layer, suggesting that we can directly discard the retrieval from current layer. However, KL divergence may occasionally fluctuate during training, making it unreliable for pruning in isolation. To address this, EBQM calibrates these divergences into a stable mapping that enables reliable identification of redundant layers. Together, these components allow ELA to reduce unnecessary computation while maintaining or even improving model accuracy.

The contributions of this paper are summarized as follows:

- We introduce a novel method that uses KL divergence to quantify redundancy in layer attention networks, enabling the identification of similar attention patterns across consecutive layers.
- We propose an innovative algorithm, Enhanced Beta Quantile Mapping (EBQM), which effectively prunes redundant attention retrievals while preserving model stability and performance.
- We present the Efficient Layer Attention (ELA) architecture, which significantly reduces computational overhead by reusing attention weights across layers, resulting in approximately 30% faster training and improved performance across tasks such as image recognition and object detection.

2 Related Work

2.1 Layer Interaction

A growing number of research has focused on enhancing layer interaction in deep convolutional neural networks. DIANet [16] introduced a parameter-shared DIA block applied across all layers to facilitate information flow throughout the network. Similarly, RLNet [41] proposed a lightweight recurrent aggregation module that efficiently reuses information from previous layers to enhance feature extraction in subsequent ones. [42] integrated features from preceding layers with the current layer using a dot product operation, sig-

nificantly boosting the model performance. BViT [18] applied an attention mechanism to the output of each layer in Vision Transformer (ViT), enabling effective integration of information across layers. ST-Unet [40] introduced a feature enhancement module at the inter-layer concatenation stage in U-Net [28], thereby improving feature extraction at each level. MRLA [8] treated features from each layer as tokens and employed an attention mechanism to promote interaction between hierarchical layers, further reinforcing the inter-layer connectivity. DLNet [33] employed a modified LSTM module at each layer to dynamically update information prior to the MRLA attention operation. Finally, MUDD [38] enhanced inter-layer interaction by dynamically adjusting connection weights based on each token’s position within a Transformer block.

2.2 Efficient Attention

Traditional attention mechanisms are often constrained by their quadratic complexity $O(n^2)$, which limits their scalability. To address this limitation, several studies have proposed more efficient alternatives. For example, [29, 22] introduced linear attention structures that significantly reduce computational overhead. Furthermore, [19] accelerated attention operations in both NLP and vision tasks by pruning tokens with low attention scores. [9] mitigated the issue of Transformers overemphasizing specific tokens by restricting the attention mechanism to a local neighborhood. SKIPAT [30] observed functional similarity across successive layers in Vision Transformers (ViTs) and proposed replacing redundant transformer blocks with lightweight parametric functions to improve efficiency. Similarly, EfficientViT [21] employed cascaded group attention to enhance attention diversity and reduce redundancy in ViTs. Additionally, [32] improved computational efficiency by pruning less important or similar tokens from the attention map.

3 Method

We start by revisiting the layer attention mechanism, followed by the motivation for our proposed Efficient Layer Attention (ELA) architecture. KL divergence is roughly employed to measure the redundant retrievals when adjacent layers attend to similar earlier layers. Then, we propose the Enhanced Beta Quantile Mapping (EBQM) algorithm, which effectively smooths the KL divergence distribution to detect and skip redundant retrievals.

3.1 Revisiting Layer Attention

Layer attention [8] enhances inter-layer interactions by employing attention mechanisms, enabling each layer to selectively retrieve relevant information from all preceding layers. Given that $\mathbf{x}^l \in \mathbb{R}^{C \times H \times W}$ represents the feature of l -th layer, where C , H , and W denote the number of channels, height, and width, respectively, we first extract the query, key, and value representations as follows:

$$\begin{cases} \mathbf{q}^l &= f_q^l(\mathbf{x}^l) \\ \mathbf{K}^l &= \text{Concat} [f_k^1(\mathbf{x}^1), \dots, f_k^l(\mathbf{x}^l)] \\ \mathbf{V}^l &= \text{Concat} [f_v^1(\mathbf{x}^1), \dots, f_v^l(\mathbf{x}^l)] \end{cases} \quad (1)$$

Here, f_q^l extracts the query \mathbf{q}^l from \mathbf{x}^l , while f_k^i and f_v^i extract the key \mathbf{k}^i and the value \mathbf{v}^i from the i -th layer, respectively. The full key and value matrices \mathbf{K}^l and \mathbf{V}^l are constructed by concatenating

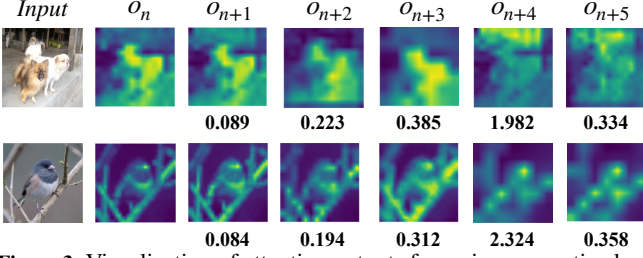


Figure 3: Visualization of attention outputs from six consecutive layers on ResNet-101. The values below each attention output (o_t) represent the KL divergence of the attention weights between the t -th and $t - 1$ -th layers.

the representations from all preceding layers up to l . Then the layer attention can be calculated as:

$$\mathbf{o}^l = \mathbf{q}^l (\mathbf{K}^l)^\top \mathbf{V}^l = \sum_{i=1}^l \mathbf{q}^l [f_k^i(\mathbf{x}^i)]^\top f_v^i(\mathbf{x}^i) \quad (2)$$

Where \mathbf{o}^l represents the l -th attention output. For clarity, the softmax and the scaling factor \mathbf{D}_k are omitted here. By substituting:

$$\mathbf{q}^l = \boldsymbol{\lambda}_o^l \odot \mathbf{q}^{l-1} \quad (3)$$

into Equation(2), a lightweight version, referred to as MRLA-L, can be derived:

$$\mathbf{o}^l = \boldsymbol{\lambda}_o^l \odot \mathbf{o}^{l-1} + \mathbf{q}^l [f_k^l(\mathbf{x}^l)]^\top f_v^l(\mathbf{x}^l) \quad (4)$$

Where $\boldsymbol{\lambda}_o^l$ is a learnable vector to dynamically adjust the contribution of prior attention output.

3.2 Motivation

In our preliminary experiments (Figure 2a), we observed that adjacent layers in layer attention networks often learn highly similar attention weights. Since layer attention retrieves information from previous layers based on these weights, such similarity leads to nearly identical attention outputs across consecutive layers. To further validate this, we employed Score-CAM [31] to visualize the attention outputs in MRLA-101. As illustrated in Figure 3, when the KL divergence between adjacent layers' attention distributions is low, their attention outputs also exhibit high visual similarity. This indicates redundant retrieval behavior—repeatedly attending to the same source of information—which not only introduces unnecessary computation but also reduces the diversity of learned features, limiting the model's representational capacity.

Motivated by these observations, we propose a method that progressively learns to skip redundant retrievals during training. Instead of recomputing attention in every layer and discarding it afterward based on KL divergence, our approach integrates redundancy detection into training itself. When the KL divergence between the current layer and the previous layer remains consistently small, the model learns to skip the attention retrieval step in subsequent layers, effectively pruning these operations from the architecture. This reduces computational overhead while improving training efficiency and maintaining expressive power.

3.3 Preliminary Knowledge

KL Divergence We first utilize the Kullback–Leibler (KL) divergence to roughly approximate the similarity between attention

weights learned in adjacent layers of a neural network. Given two discrete probability distributions $P = \{p_1, \dots, p_n\}$ and $Q = \{q_1, \dots, q_n\}$, the KL divergence is defined as:

$$D_{\text{KL}}(P \parallel Q) = \sum_i p_i \log \left(\frac{p_i}{q_i} \right) \quad (5)$$

The KL divergence measures the difference between two distributions: a smaller value implies higher similarity, while a larger value indicates greater divergence.

KL Divergence in Layer Attention The output of the l -th layer \mathbf{x}^l can be expressed as a linear combination of value vectors:

$$\mathbf{x}^l = p_1 v_1 + \dots + p_l v_l \quad (6)$$

where $v_i = f_v^i(\mathbf{x}^i)$ is the i -th value in \mathbf{V}^l , and $P = \{p_1, \dots, p_l\}$ denotes the attention weight from l -th layer, which can be interpreted as a probability distribution.

Similarly, the output of the $l + 1$ -th layer \mathbf{x}^{l+1} can be written as:

$$\mathbf{x}^{l+1} = p'_1 v_1 + \dots + p'_{l+1} v_{l+1} \quad (7)$$

where $P' = \{p'_1, \dots, p'_{l+1}\}$ is the attention weight derived from $l + 1$ -th layer. Notably, the distribution P' contains one additional term, p'_{l+1} , compared to P .

To enable a valid comparison between the two distributions, we pad P with an infinitesimal value ϵ (where $\epsilon \rightarrow 0$), resulting in $P = \{p_1, \dots, p_l, \epsilon\}$, so that its dimensionality matches that of P' .

The KL divergence between the two distributions is then computed as:

$$D_{\text{KL}}(P \parallel P') = \sum_{i=1}^l p_i \log \left(\frac{p_i}{p'_i} \right) + \epsilon \log \left(\frac{\epsilon}{p'_{l+1}} \right) \quad (8)$$

In a layer attention network, the previous values v_1, \dots, v_{l+1} remain consistent between layers l and $l + 1$. Consequently, the difference between the outputs \mathbf{x}^l and \mathbf{x}^{l+1} is solely attributed to the change in their corresponding attention weight distributions, P and P' . Therefore, the KL divergence between P and P' directly captures the degree of similarity between the two outputs.

3.4 Efficient Layer Attention

ELA Architecture We present the details of our proposed Efficient Layer Attention (ELA) architecture (Shown in Figure 1). Firstly, we compute the KL divergences between attention weights learned from all adjacent layers using Equation (8), and collect the results into a divergence vector $\mathbf{a} = (a_1, \dots, a_{L-1})$. This vector is then passed through the EBQM module $\mathcal{E}()$, which smooths the divergence values as follows:

$$\tilde{\mathbf{a}} = \mathcal{E}(\mathbf{a}) = (\tilde{a}_1, \dots, \tilde{a}_{L-1}) \quad (9)$$

Next, we apply a pruning mechanism based on a pre-defined threshold τ . A binary mask $\mathbf{m} = (m_1, \dots, m_L)$ is generated as:

$$\begin{cases} m_1 &= 1 \\ m_{l+1} &= 1[\tilde{a}_l \geq \tau] \in \{0, 1\} \quad l = 1, \dots, L - 1 \end{cases}$$

This mask determines whether the attention outputs from each layer should be preserved or pruned. In each layer l , the representations of query, key, and value are then updated as follows:

$$\begin{cases} \mathbf{q}^l &= f_q^l(\mathbf{x}^l) \\ \mathbf{K}^l &= \text{Concat}[m_1 f_k^1(\mathbf{x}^1), \dots, m_l f_k^l(\mathbf{x}^l)] \\ \mathbf{V}^l &= \text{Concat}[m_1 f_v^1(\mathbf{x}^1), \dots, m_l f_v^l(\mathbf{x}^l)] \end{cases} \quad (10)$$

Then refined query \mathbf{q}^l , \mathbf{K}^l and \mathbf{V}^l are then used to compute the layer attention for layer l as described in Equation (2).

Training Strategies Our training process is divided into multiple stages. At the beginning of each stage, we compute the KL divergences between the attention weights of adjacent MRLA layers. Notably, we do not predefine a fixed number of layers to skip. This is because the KL divergence distribution at each stage (except the initial one) is influenced by the pruning results from previous stages, which dynamically affects the number of layers to be discarded. If a fixed number of layers were removed at each stage, important attention layers might be pruned in some stages, ultimately degrading model performance—as evidenced by the results in Table 4. However, within each stage, the KL divergence distribution remains relatively stable.

3.5 EBQM Algorithm

The proposed pruning approach, detailed in Algorithm 1, leverages a threshold μ to determine which layers to discard. Initially, we focus on the KL divergence values that fall below the γ -quantile and normalize these values to the range $x \in [0, 1]$ to simplify thresholding. However, these normalized values are often tightly clustered, making the pruning highly sensitive to small variations across training runs. For example, with a threshold $\mu = 0.3$, six layers with KL divergences between 0.31 and 0.33 in one run may shift to between 0.27 and 0.29 in another. This results in up to six fewer skipped layers in the latter case, introducing inconsistencies that can significantly impact model performance and robustness, as shown in Table 4.

Algorithm 1 Enhanced Beta Quantile Mapping (EBQM)

Input: KL divergences from layer 1 to layer l : $[a_1, a_2, \dots, a_l]$

Parameter: Quantile γ , Beta distribution parameters α, β , threshold ϵ , number of epochs E

Output: Updated KL divergences $[\tilde{a}_1, \dots, \tilde{a}_{L-1}]$ with skipped layers

1: **for** epoch $e = 1$ to E **do**

2: Sort KL divergences in ascending order:

$$[a_1, a_2, \dots, a_l] \rightarrow [a_{(1)}, a_{(2)}, \dots, a_{(l)}]$$

$$a_{(1)} \leq a_{(2)} \leq \dots \leq a_{(l)}$$

3: Extract γ -quantile:

$$S_\gamma = \{a_i \mid a_i \leq Q_\gamma\}, \quad Q_\gamma = \gamma\text{-quantile of } [a_1, \dots, a_l]$$

4: **for** each $a_j \in S_\gamma$ **do**

5: Normalize a_j :

$$a'_j = \frac{a_j - \min(S_\gamma)}{\max(S_\gamma) - \min(S_\gamma)}$$

6: Apply Beta CDF: $b_j = F_{\text{Beta}}(a'_j; \alpha, \beta)$

7: **end for**

8: **end for**

9: **return** Updated KL divergences $[\tilde{a}_1, \dots, \tilde{a}_{L-1}]$

To mitigate this issue, we propose preprocessing the normalized KL divergence distribution before thresholding. Drawing inspiration from the Quantile Mapping Algorithm—a technique widely used in meteorology and hydrology to adjust data distributions—we introduce the **Enhanced Beta Quantile Mapping (EBQM)** algorithm. EBQM reshapes the distribution using the cumulative distribution function (CDF) of the Beta distribution.

The CDF of the Beta distribution is defined as:

$$\text{CDF}_{\text{Beta}}(x) = \begin{cases} 0 & \text{if } x < 0 \\ F_{\text{Beta}}(x; \alpha, \beta) & \text{if } 0 \leq x \leq 1 \\ 1 & \text{if } x > 1 \end{cases}$$

where $F_{\text{Beta}}(x; \alpha, \beta)$ is given by:

$$F_{\text{Beta}}(x; \alpha, \beta) = \int_0^x \frac{t^{\alpha-1}(1-t)^{\beta-1}}{B(\alpha, \beta)} dt \quad (11)$$

and $B(\alpha, \beta)$ is the Beta function:

$$B(\alpha, \beta) = \int_0^1 t^{\alpha-1}(1-t)^{\beta-1} dt \quad (12)$$

Unlike other distributions such as the Gamma distribution, the Beta distribution's CDF is strictly defined within the $[0, 1]$ interval for both its input and output. This makes it especially suitable for transforming normalized KL divergence values, which also lie within $[0, 1]$. By applying this transformation and tuning the shape parameters α and β , we can effectively spread out tightly clustered values, enabling more stable and robust pruning decisions across different training stages.

4 Experiments

4.1 Image Classification

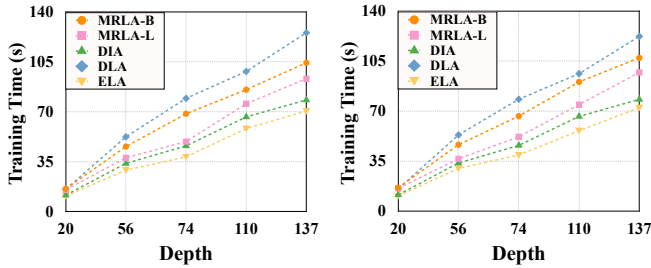
We carried out experiments on the CIFAR-10, CIFAR-100, and ImageNet-1K [6] datasets, utilizing ResNet [10] as the backbone compared with various baselines, such as channel attention methods, spatial attention models, and other layer interaction methods. For the CIFAR-10 and CIFAR-100 datasets, we applied the data augmentation techniques described in [14]. For the ImageNet-1K dataset, the augmentation techniques and hyperparameter configurations followed those specified by [10, 11].

Experimental Settings When training on CIFAR-10 and CIFAR-100 datasets, α and β were set to 5 and 1, respectively, and μ set to 0.3. We trained for a total of 180 epochs, averaging the KL divergence values from the first to the third epoch to determine the final data to discard. This process was repeated during the 45th to 48th epochs and again during the 91st to 93rd epochs. Furthermore, the model was trained on ImageNet-1K for 100 epochs. The KL divergence values were averaged over the first to third epochs and the 51st to 53rd epochs to guide layer pruning. Consistent with the CIFAR settings, α and β were set to 2 and 5, respectively, with the threshold μ adjusted to 0.25.

Results on CIFAR-10 and CIFAR-100 ELANet, which integrates the proposed method of pruning attention operations from certain layers, demonstrates a clear advantage over baseline models on both CIFAR-10 and CIFAR-100. As shown in Table 1, ELA achieves 93.13% and 72.07% top-1 accuracy on the ResNet-20 backbone, surpassing ResNet-20 by 1.78% and 4.12% on CIFAR-10 and CIFAR-100, respectively. ELA also outperforms several channel and spatial attention models, such as SE [13], BAM [24], and CBAM [37].

Data	CIFAR-10		CIFAR-100	
Models	Params	Top-1	Params	Top-1
ResNet-20	0.22M	91.35	0.24M	67.95
SE	0.24M	91.22	0.27M	68.61
ECA	0.22M	91.45	0.24M	67.35
DIA	0.44M	92.02	0.46M	68.83
CBAM	0.24M	91.97	0.27M	67.71
BAM	0.27M	91.87	0.29M	67.91
MRLA-L	0.23M	92.21	0.25M	70.84
CAA	0.59M	92.32	0.61M	71.21
SHSA	0.41M	92.27	0.43M	71.64
DLA	0.41M	92.68	0.43M	71.44
ELA	0.23M	93.13	0.25M	72.07
ResNet-56	0.59M	93.01	0.61M	72.36
SE	0.66M	93.56	0.68M	73.78
ECA	0.59M	94.11	0.61M	73.38
DIA	0.81M	93.56	0.83M	74.01
CBAM	0.66M	93.76	0.68M	73.71
BAM	0.73M	93.44	0.75M	73.64
MRLA-L	0.62M	93.88	0.64M	74.13
CAA	1.70M	94.17	1.72M	74.38
SHSA	1.15M	94.09	1.17M	74.23
DLA	0.80M	94.52	0.82M	74.79
ELA	0.62M	94.89	0.64M	75.48
ResNet-110	1.15M	92.94	1.17M	73.04
SE	1.28M	94.30	1.30M	75.18
ECA	1.15M	94.27	1.17M	75.08
DIA	1.37M	94.13	1.39M	75.14
CBAM	1.28M	93.79	1.30M	74.87
BAM	1.42M	93.84	1.45M	74.99
MRLA-L	1.21M	94.14	1.23M	75.02
CAA	3.37M	94.22	3.39M	75.22
SHSA	2.27M	93.76	2.29M	75.31
DLA	1.39M	94.36	1.41M	75.69
ELA	1.21M	95.08	1.23M	76.25

Table 1: Top-1 accuracy (%) of different models with ResNet backbone on CIFAR-10 and CIFAR-100.



(a) Training Time on CIFAR-10

(b) Training Time on CIFAR-100

Figure 4: Comparison of per epoch training time (in seconds) for different layer interaction models with varying depths under identical training conditions.

In the ResNet-56 backbone, ELA surpasses SE, BAM, and CBAM by 1.51%, 1.63%, and 1.31% on CIFAR-10, and by 1.70%, 1.84%, and 1.77% on CIFAR-100, respectively, with lower parameters introduced. Furthermore, in ResNet-110, our model exceeds a number of layer interaction models, surpassing DIA[16] and MRLA-L [8] by 0.95% and 0.94% on CIFAR-10, and by 1.11% and 1.23% on CIFAR-100, respectively. ELA also outperforms recent attention mechanisms such as CAA [2] and SHSA [39], surpassing them by 0.81 and 0.86 on CIFAR-10, and by 0.86% and 0.43% on CIFAR-100 in ResNet-20, respectively. In ResNet-56 and ResNet-110, ELA

also exceeds Dynamic Layer Attention (DLA) [33], achieving improvements of 0.37% and 0.72% in CIFAR-10 and 0.69% and 0.76% in CIFAR-100. These results highlight ELA’s superior classification performance while maintaining efficient parameter usage across various network depths.

ELA significantly reduces training time. As shown in Figure 4, the training time for the five layer attention networks on CIFAR-10 and CIFAR-100 are nearly identical for one epoch, with DLA exhibiting the longest training time. Compared to MRLA-B, MRLA-L reduces training time by approximately 10%-15%, while the proposed ELA achieves an even greater reduction, decreasing training time by around 30%-35% relative to the original MRLA-B. ELA also reduces training time by 5% to 7% compared to DIA, the most lightweight layer interaction network to date. Moreover, the reduction in training time of ELA becomes more significant as the number of network layers increases.

Models	Params	FLOPs	Top-1	Top-5
ResNet-50	25.6M	4.1B	76.1	92.9
SE	28.1M	4.1B	76.7	93.4
CBAM	28.1M	4.2B	77.3	93.7
A^2	34.6M	7.0B	77.0	93.5
AA	27.1M	4.5B	77.7	93.8
GC	29.4M	4.2B	77.7	93.7
ECA	25.6M	4.1B	77.5	93.7
RLA	25.9M	4.5B	77.2	93.4
MRLA-L	25.7M	4.2B	77.7	93.8
MRLA-B	25.7M	4.6B	77.7	93.9
DLA	27.2M	4.3B	77.8	94.0
S6LA	25.8M	4.4B	78.0	94.2
ELA	25.7M	4.4B	78.1	94.4
ResNet-101	44.5M	7.8B	77.4	93.5
SE	49.3M	7.8B	77.6	93.9
CBAM	49.3M	7.9B	78.5	94.3
AA	47.6M	8.6B	78.7	94.4
ECA	44.5M	7.8B	78.7	94.3
RLA	45.0M	8.4B	78.5	94.2
MRLA-L	44.9M	7.9B	78.7	94.4
DLA	47.8M	8.1B	78.8	94.5
ELA	44.9M	8.1B	79.1	94.6

Table 2: Top-1 and Top-5 accuracy (%) of different models with ResNet backbone on ImageNet-1K.

Results on ImageNet-1K We compare ELA with a range of state-of-the-art models, using ResNet as backbone. As shown in Table 2, ELA achieves 78.1% Top-1 accuracy on the ResNet-50, an improvement of 2.0% over its backbone. Compared to attention-based models like SE and CBAM, ELA offers 1.4% and 0.8% higher Top-1 accuracy, respectively, while using a smaller number of parameters. Moreover, ELA outperforms A^2 [5] by 1.1%, AA [1] by 0.4%, and GC [3] by 0.4%. Furthermore, ELA performs better than MRLA-L, which achieves 77.7%, by 0.4% in the accuracy of Top-1. For the deeper ResNet-101 backbone, ELA again delivers the best performance, achieving 79.1% in Top-1 accuracy, surpassing ResNet-101 by 1.7%. It also outperforms SE, CBAM, and AA by 0.5%, 0.6%, and 0.4%, respectively. Notably, ELA achieves 0.4% higher Top-1 accuracy than MRLA-L, which reaches 78.7%. When compared to lightweight models such as ECA, ELA provides an additional 0.6% improvement in Top-1 accuracy for ResNet-50 and 0.4% for ResNet-101, despite a slight increase in parameters. Moreover, compared to the latest layer interaction networks DLA and S6LA [20], ELA

Detectors	Methods	Params	AP	AP ₅₀	AP ₇₅	AP _S	AP _M	AP _L
Faster R-CNN	ResNet-50	41.5M	36.4	58.2	39.2	21.8	40.0	46.2
	SE	44.0M	37.7	60.1	40.9	22.9	41.9	48.2
	ECA	41.5M	38.0	60.6	40.9	23.4	42.1	48.0
	RLA	41.8M	38.8	59.6	42.0	22.5	42.9	49.5
	MRLA-L	41.7M	40.1	61.3	43.8	24.0	43.9	52.2
	DLA	44.2M	40.3	61.6	43.9	24.1	44.2	52.7
	S6LA	42.2M	40.3	61.7	43.8	24.2	44.0	52.5
	ELA	41.7M	40.7	61.7	44.4	24.6	44.2	52.9
	ResNet-101	60.5M	38.7	60.6	41.9	22.7	43.2	50.4
	SE	65.2M	39.6	62.0	43.1	23.7	44.0	51.4
	ECA	60.5M	40.3	62.9	44.0	24.5	44.7	51.3
	RLA	60.9M	41.2	61.8	44.9	23.7	45.7	53.8
	MRLA-L	60.9M	41.3	62.9	45.0	24.7	45.5	53.8
	DLA	63.4 M	42.0	63.3	45.1	24.8	45.9	55.0
	S6LA	61.3M	41.7	63.0	45.2	24.6	45.6	53.9
	ELA	60.9M	42.1	63.3	45.8	25.2	45.9	55.5
Mask R-CNN	ResNet-50	44.2M	37.2	58.9	40.3	34.1	55.5	36.2
	SE	46.7M	38.7	60.9	42.1	35.4	57.4	37.8
	ECA	44.2M	39.0	61.3	42.1	35.6	58.1	37.7
	NL	46.5M	38.0	59.8	41.0	34.7	56.7	36.6
	GC	46.9M	39.4	61.6	42.4	35.7	58.4	37.6
	RLA	44.4M	39.5	60.1	43.4	35.6	56.9	38.0
	MRLA-L	44.3M	40.4	61.8	44.0	36.9	57.8	38.3
	DLA	46.9M	40.9	62.0	44.7	37.0	58.8	39.0
	S6LA	44.9M	40.6	61.5	44.2	36.7	58.3	38.3
	ELA	44.3M	41.4	62.4	45.2	37.3	59.2	39.8
	ResNet-101	63.2M	39.4	60.9	43.3	35.9	57.7	38.4
	SE	67.9M	40.7	62.5	44.3	36.8	59.3	39.2
	ECA	63.2M	41.3	63.1	44.8	37.4	59.9	39.8
	NL	65.5M	40.8	63.1	44.5	37.1	59.9	39.2
	GC	82.2M	41.7	63.7	45.5	37.6	60.5	39.8
	RLA	63.6M	41.8	62.3	46.2	37.3	59.2	40.1
	MRLA-L	63.5M	42.5	63.3	46.1	38.1	60.3	40.6
	DLA	66.1M	42.6	63.5	46.4	38.2	60.5	40.9
	S6LA	64.0 M	42.7	63.3	46.2	38.3	60.5	41.0
	ELA	63.5M	42.9	63.7	46.7	38.6	60.7	41.2

Table 3: Object detection results on the COCO2017 dataset using various methods with Mask R-CNN and Faster R-CNN detectors

achieves performance gains of 0.3% and 0.1% on ResNet-50, respectively. The results demonstrate that ELA significantly outperforms other models in terms of Top-1 and Top-5 accuracy, while maintaining competitive computational efficiency.

4.2 Object Detection

Experimental Settings In the object detection task, our approach was evaluated on the COCO2017 dataset using Faster R-CNN and Mask R-CNN as detectors. All models were implemented using the open-source MMDetection toolkit [4] to ensure consistency and reproducibility, with all configurations following the default MMDetection settings. Each detector underwent 12 training epochs, with KL divergence measured at the 1st epoch and 7th epoch to analyze layer significance at early and later training stages. The hyperparameters α and β were set to 2 and 5, respectively, while μ was fixed at 0.2.

Results on COCO2017 Our proposed ELA method achieves significant improvements in object detection performance compared to several state-of-the-art methods across various backbone networks and detectors. As highlighted in Table 3, when Faster R-CNN is used with ResNet-50, ELA outperforms SE, ECA, and RLA [41] by achieving 40.7% in AP, a gain of 3.0% over SE and 2.7% over ECA and 1.9% over RLA. It also shows improvements in AP₅₀ and AP₇₅, highlighting its superiority in detecting objects across different scales. With ResNet-101, ELA continues to show competitive performance, surpassing not only MRLA-L, but also SE, ECA, and other models, with

a 0.1% improvement in AP and a notable increase in AP₅₀ and AP₇₅. Similarly, when Mask R-CNN is used as the detector, ELA maintains its edge, achieving a 1.0% increase in AP compared to MRLA-L on ResNet-50, and showing substantial improvements over methods like NL [35] and GC [3]. Moreover, ELA achieves state-of-the-art performance compared to recent layer interaction networks, such as DLA and S6LA, on both Faster R-CNN and Mask R-CNN, while maintaining the lowest parameter count. These results confirm that ELA consistently enhances object detection accuracy, offering a balanced trade-off between performance and computational efficiency.

5 Ablation Studies

5.1 Evaluation of Different Layer Pruning Methods

To evaluate the effectiveness of EBQM, we conducted comparative experiments with two alternative strategies. First, a fixed layer pruning strategy was employed, where the number of pruned layers was determined by a hyperparameter. The pruned layer count was aligned as closely as possible with the number determined by Algorithm 1. Second, a threshold-based pruning strategy was implemented, using a fixed hyperparameter to define a KL divergence threshold: layers with values below the threshold were discarded, while those above were retained. The ablation experiments were conducted on CIFAR-100 using ResNet [10] architectures of varying depths as baselines. Each experiment was repeated five times, and results were reported as *Accuracy \pm Standard Deviation* to evaluate the model’s robustness and performance.

Depth	Methods	Top-1
56	Threshold-Based	74.36±0.44
	Fixed Layer Pruning	74.29±0.30
	EBQM	75.48±0.24
110	Threshold-Based	74.83±0.79
	Fixed Layer Pruning	74.92±0.41
	EBQM	76.25±0.22

Table 4: Top-1 accuracy (%) of different methods for redundant layer pruning with ResNet backbone on CIFAR-100.

As shown in Table 4, it is evident that as the network depth increases, the instability of the Threshold-Based method also increases. The standard deviation rises from 0.44% in ResNet-56 to 0.79% in ResNet-110. A similar trend is observed with the Fixed Layer Pruning method. In contrast, the Top-1 accuracy achieved by our EBQM is consistently higher than that of the other two methods, reaching 75.48% and 76.25% for ResNet-56 and ResNet-110, respectively.

5.2 Evaluation of Different Quantile Mapping Algorithms

To evaluate the performance of EBQM in comparison to existing quantile mapping algorithms, we compared EBQM with widely used gamma quantile mapping (GQM) methods [25] and exponential quantile mapping (EQM) methods [12].

Depth	Algorithms	Top-1
56	GQM	74.02±0.38
	EQM	73.93±0.34
	EBQM	75.48±0.24
110	GQM	74.98±0.41
	EQM	75.05±0.37
	EBQM	76.25±0.22

Table 5: Top-1 accuracy (%) of different quantile mapping algorithms with ResNet backbone on CIFAR-100.

EBQM surpasses both GQM and EQM in Top-1 accuracy, achieving 75.48% and 76.25% for ResNet-56 and ResNet-110, respectively, as demonstrated in Table 5. These results surpass those of GQM, with accuracies of 74.02% and 74.98%, and EQM, with accuracies of 73.93% and 75.05%. Moreover, EBQM demonstrates the lowest standard deviation, at 0.24% and 0.22%, indicating superior stability when compared to GQM and EQM.

5.3 Evaluation of Different Distributions and Activation Functions in EBQM

We also investigated whether the selection of the Beta distribution in EBQM outperforms other distributions or activation functions. To this end, we replaced the Beta distribution with commonly used alternatives, such as the Gamma and Normal distributions, as well as activation functions like Softmax and Sigmoid.

Depth	Distributions	Top-1
56	Normal	73.92±0.39
	Gamma	74.11±0.33
	Beta	75.48±0.24
110	Normal	74.89±0.44
	Gamma	75.12±0.34
	Beta	76.25±0.22

Table 6: Top-1 accuracy (%) of different kinds of distributions and activation functions in EBQM with ResNet backbone on CIFAR-100.

The Beta distribution outperforms both the Normal and Gamma distributions, as well as the Softmax and Sigmoid functions, in terms of Top-1 accuracy, achieving 75.48% and 76.25% for ResNet-56 and ResNet-110, respectively, as shown in Table 6. Furthermore, the Beta distribution exhibits superior stability, with the lowest standard deviations of 0.24% and 0.22%, indicating more consistent performance compared to the other distributions.

6 Conclusion

In this paper, we uncover the inherent redundancy in existing layer attention mechanisms, characterized by the high similarity of attention weights learned by adjacent layers. We further analyze the two key issues caused by this redundancy: degraded model performance and extended training time. To address these challenges, we propose a novel approach that first evaluates the importance of each attention layer using KL divergence and then employs an Enhanced Beta Quantile Mapping Algorithm to prune redundant layers. Experimental results on image classification and object detection tasks demonstrate that our method effectively eliminates redundant information, resulting in a network that outperforms the original layer attention model.

References

- [1] I. Bello, B. Zoph, A. Vaswani, J. Shlens, and Q. V. Le. Attention augmented convolutional networks. In *Proceedings of the IEEE/CVF international conference on computer vision*, pages 3286–3295, 2019.
- [2] X. Cai, Q. Lai, Y. Wang, W. Wang, Z. Sun, and Y. Yao. Poly kernel inception network for remote sensing detection. In *Proceedings of the IEEE/CVF Conference on Computer Vision and Pattern Recognition (CVPR)*, pages 27706–27716, June 2024.
- [3] Y. Cao, J. Xu, S. Lin, F. Wei, and H. Hu. Gcnet: Non-local networks meet squeeze-excitation networks and beyond. In *Proceedings of the IEEE/CVF international conference on computer vision workshops*, pages 0–0, 2019.
- [4] K. Chen, J. Wang, J. Pang, Y. Cao, Y. Xiong, X. Li, S. Sun, W. Feng, Z. Liu, J. Xu, et al. Mmdetection: Open mmlab detection toolbox and benchmark. *arXiv preprint arXiv:1906.07155*, 2019.
- [5] Y. Chen, Y. Kalantidis, J. Li, S. Yan, and J. Feng. A²-nets: Double attention networks. *Advances in neural information processing systems*, 31, 2018.
- [6] J. Deng, W. Dong, R. Socher, L.-J. Li, K. Li, and L. Fei-Fei. Imagenet: A large-scale hierarchical image database. In *2009 IEEE conference on computer vision and pattern recognition*, pages 248–255. Ieee, 2009.
- [7] A. Dosovitskiy. An image is worth 16x16 words: Transformers for image recognition at scale. *arXiv preprint arXiv:2010.11929*, 2020.
- [8] Y. Fang, Y. Cai, J. Chen, J. Zhao, G. Tian, and G. Li. Cross-layer retrospective retrieving via layer attention. *arXiv preprint arXiv:2302.03985*, 2023.
- [9] Y. Guo, D. Stutz, and B. Schiele. Robustifying token attention for vision transformers. In *Proceedings of the IEEE/CVF International Conference on Computer Vision*, pages 17557–17568, 2023.
- [10] K. He, X. Zhang, S. Ren, and J. Sun. Deep residual learning for image recognition. In *Proceedings of the IEEE conference on computer vision and pattern recognition*, pages 770–778, 2016.
- [11] T. He, Z. Zhang, H. Zhang, Z. Zhang, J. Xie, and M. Li. Bag of tricks for image classification with convolutional neural networks. In *Proceedings of the IEEE/CVF conference on computer vision and pattern recognition*, pages 558–567, 2019.
- [12] J.-H. Heo, H. Ahn, J.-Y. Shin, T. R. Kjeldsen, and C. Jeong. Probability distributions for a quantile mapping technique for a bias correction of precipitation data: A case study to precipitation data under climate change. *Water*, 11(7):1475, 2019.
- [13] J. Hu, L. Shen, and G. Sun. Squeeze-and-excitation networks. In *Proceedings of the IEEE conference on computer vision and pattern recognition*, pages 7132–7141, 2018.
- [14] G. Huang, Y. Sun, Z. Liu, D. Sedra, and K. Q. Weinberger. Deep networks with stochastic depth. In *Computer Vision—ECCV 2016: 14th European Conference, Amsterdam, The Netherlands, October 11–14, 2016, Proceedings, Part IV 14*, pages 646–661. Springer, 2016.

- [15] G. Huang, Z. Liu, L. Van Der Maaten, and K. Q. Weinberger. Densely connected convolutional networks. In *Proceedings of the IEEE conference on computer vision and pattern recognition*, pages 4700–4708, 2017.
- [16] Z. Huang, S. Liang, M. Liang, and H. Yang. Dianet: Dense-and-implicit attention network. In *Proceedings of the AAAI Conference on Artificial Intelligence*, volume 34, pages 4206–4214, 2020.
- [17] J. Li, Y. Wen, and L. He. Scconv: Spatial and channel reconstruction convolution for feature redundancy. In *Proceedings of the IEEE/CVF Conference on Computer Vision and Pattern Recognition*, pages 6153–6162, 2023.
- [18] N. Li, Y. Chen, W. Li, Z. Ding, D. Zhao, and S. Nie. Bvit: Broad attention-based vision transformer. *IEEE Transactions on Neural Networks and Learning Systems*, 2023.
- [19] Z. Li, S. Ghodrati, A. Yazdanbakhsh, H. Esmaeilzadeh, and M. Kang. Accelerating attention through gradient-based learned runtime pruning. In *Proceedings of the 49th Annual International Symposium on Computer Architecture*, pages 902–915, 2022.
- [20] Q. Liu, W. Zhao, W. Huang, Y. Fang, L. Yu, and G. Li. From layers to states: A state space model perspective to deep neural network layer dynamics. *arXiv preprint arXiv:2502.10463*, 2025.
- [21] X. Liu, H. Peng, N. Zheng, Y. Yang, H. Hu, and Y. Yuan. Efficientvit: Memory efficient vision transformer with cascaded group attention. In *Proceedings of the IEEE/CVF Conference on Computer Vision and Pattern Recognition*, pages 14420–14430, 2023.
- [22] X. Ma, X. Kong, S. Wang, C. Zhou, J. May, H. Ma, and L. Zettlemoyer. Luna: Linear unified nested attention. *Advances in Neural Information Processing Systems*, 34:2441–2453, 2021.
- [23] D. Ouyang, S. He, G. Zhang, M. Luo, H. Guo, J. Zhan, and Z. Huang. Efficient multi-scale attention module with cross-spatial learning. In *ICASSP 2023-2023 IEEE International Conference on Acoustics, Speech and Signal Processing (ICASSP)*, pages 1–5. IEEE, 2023.
- [24] J. Park. Bam: Bottleneck attention module. *arXiv preprint arXiv:1807.06514*, 2018.
- [25] C. Piani, J. Haerter, and E. Coppola. Statistical bias correction for daily precipitation in regional climate models over europe. *Theoretical and applied climatology*, 99:187–192, 2010.
- [26] W. Qian and H. H. Chang. Projecting health impacts of future temperature: a comparison of quantile-mapping bias-correction methods. *International journal of environmental research and public health*, 18(4):1992, 2021.
- [27] Z. Qin, P. Zhang, F. Wu, and X. Li. Fcanet: Frequency channel attention networks. In *Proceedings of the IEEE/CVF international conference on computer vision*, pages 783–792, 2021.
- [28] O. Ronneberger, P. Fischer, and T. Brox. U-net: Convolutional networks for biomedical image segmentation. In *Medical image computing and computer-assisted intervention—MICCAI 2015: 18th international conference, Munich, Germany, October 5–9, 2015, proceedings, part III* 18, pages 234–241. Springer, 2015.
- [29] Z. Shen, M. Zhang, H. Zhao, S. Yi, and H. Li. Efficient attention: Attention with linear complexities. In *Proceedings of the IEEE/CVF winter conference on applications of computer vision*, pages 3531–3539, 2021.
- [30] S. Venkataramanan, A. Ghodrati, Y. M. Asano, F. Porikli, and A. Habibiian. Skip-attention: Improving vision transformers by paying less attention. *arXiv preprint arXiv:2301.02240*, 2023.
- [31] H. Wang, Z. Wang, M. Du, F. Yang, Z. Zhang, S. Ding, P. Mardziel, and X. Hu. Score-cam: Score-weighted visual explanations for convolutional neural networks. In *Proceedings of the IEEE/CVF conference on computer vision and pattern recognition workshops*, pages 24–25, 2020.
- [32] H. Wang, B. Dedhia, and N. K. Jha. Zero-tprune: Zero-shot token pruning through leveraging of the attention graph in pre-trained transformers. In *Proceedings of the IEEE/CVF Conference on Computer Vision and Pattern Recognition*, pages 16070–16079, 2024.
- [33] K. Wang, X. Xia, J. Liu, Z. Yi, and T. He. Strengthening layer interaction via dynamic layer attention. *arXiv preprint arXiv:2406.13392*, 2024.
- [34] Q. Wang, B. Wu, P. Zhu, P. Li, W. Zuo, and Q. Hu. Eca-net: Efficient channel attention for deep convolutional neural networks. In *Proceedings of the IEEE/CVF conference on computer vision and pattern recognition*, pages 11534–11542, 2020.
- [35] X. Wang, R. Girshick, A. Gupta, and K. He. Non-local neural networks. In *Proceedings of the IEEE conference on computer vision and pattern recognition*, pages 7794–7803, 2018.
- [36] Y. Wang, Y. Li, G. Wang, and X. Liu. Multi-scale attention network for single image super-resolution. In *Proceedings of the IEEE/CVF Conference on Computer Vision and Pattern Recognition*, pages 5950–5960, 2024.
- [37] S. Woo, J. Park, J.-Y. Lee, and I. S. Kweon. Cbam: Convolutional block attention module. In *Proceedings of the European conference on computer vision (ECCV)*, pages 3–19, 2018.
- [38] D. Xiao, Q. Meng, S. Li, and X. Yuan. Muddformer: Breaking residual bottlenecks in transformers via multiway dynamic dense connections. *arXiv preprint arXiv:2502.12170*, 2025.
- [39] S. Yun and Y. Ro. Shvit: Single-head vision transformer with memory efficient macro design. In *Proceedings of the IEEE/CVF Conference on Computer Vision and Pattern Recognition*, pages 5756–5767, 2024.
- [40] J. Zhang, Q. Qin, Q. Ye, and T. Ruan. St-unet: Swin transformer boosted u-net with cross-layer feature enhancement for medical image segmentation. *Computers in Biology and Medicine*, 153:106516, 2023.
- [41] J. Zhao, Y. Fang, and G. Li. Recurrence along depth: Deep convolutional neural networks with recurrent layer aggregation. *Advances in Neural Information Processing Systems*, 34:10627–10640, 2021.
- [42] Y. Zhao, J. Chen, Z. Zhang, and R. Zhang. Ba-net: Bridge attention for deep convolutional neural networks. In *European Conference on Computer Vision*, pages 297–312. Springer, 2022.

Appendices

A Quantile Mapping

Algorithm 2 Quantile Mapping Algorithm

Input: A numerical set $\mathbf{X} = \{x_1, x_2, \dots, x_n\}$

Parameter: Target distribution F_θ with parameter θ

Output: Transformed set \mathbf{X}'

1: Compute the empirical cumulative probability for each x_i :

$$p(x_i) = \frac{1}{n} \sum_{j=1}^n \mathbb{I}(x_j \leq x_i), \quad p(x_i) \in [0, 1],$$

where $\mathbb{I}(\cdot)$ is the indicator function.

2: **for** $x_i \in \mathbf{X}$ **do**

3: Apply quantile mapping:

$$x'_i = F_\theta^{-1}(p(x_i)),$$

where F_θ^{-1} is the inverse CDF of the target distribution F_θ .

4: **end for**

5: **return** $\mathbf{X}' = \{x'_1, x'_2, \dots, x'_n\}$

Algorithm 2 outlines the original Quantile Mapping Algorithm as introduced by [26]. In this method, the Gamma distribution and Exponential distribution are frequently utilized to model the target distribution F_θ . Their cumulative distribution functions (CDFs) are as follows:

The CDF of the Gamma distribution is given by:

$$F_{\text{Gamma}}(x; \alpha, \beta) = \int_0^x \frac{t^{\alpha-1} e^{-t/\beta}}{\Gamma(\alpha) \beta^\alpha} dt$$

where α is the shape parameter, β is the scale parameter, and $\Gamma(\alpha)$ is the Gamma function, which is defined as:

$$\Gamma(\alpha) = \int_0^\infty t^{\alpha-1} e^{-t} dt$$

The CDF of the Exponential distribution is given by:

$$F_{\text{Exp}}(x; \lambda) = 1 - e^{-\lambda x}$$

where λ is the rate parameter of the distribution.

B Visualization

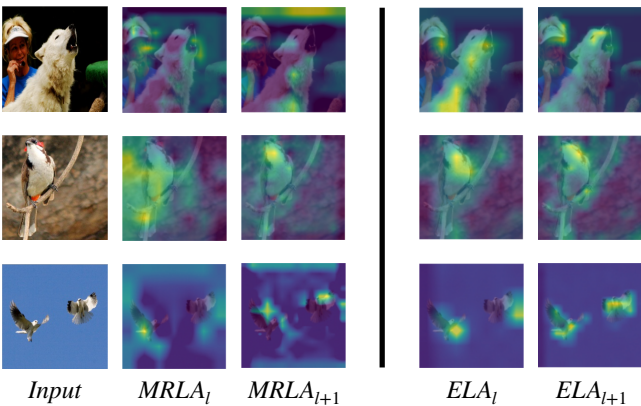


Figure 5

Figure 5 illustrates a comparison of the feature maps before and after the removal of redundant attention layers. The l -th and $l+1$ -th layers represent the attention layers identified for removal. It can be observed that by removing the MRLA layer while preserving the original ResNet backbone structure, the features extracted by these layers exhibit significant differences. Furthermore, it is evident that in certain layers, the removal of attention leads to the extraction of more precise features, thereby enhancing the model's representational capacity.

Figures 6 and 7 show the attention maps of MRLA on the CIFAR-100 dataset with ResNet-56 and the ImageNet-1K dataset with ResNet-50, respectively.

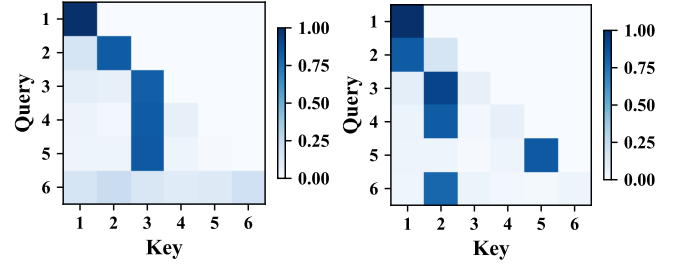


Figure 6: Visualization of attention scores at different stages of layer attention on the ResNet-56 backbone for CIFAR-100.

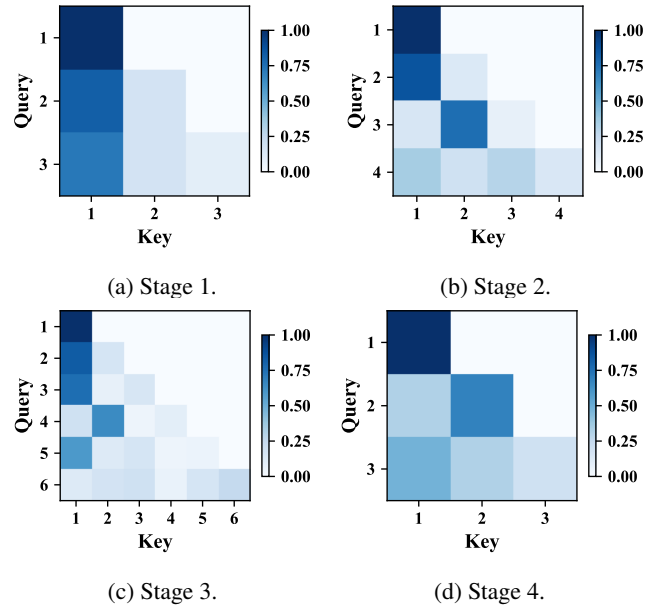


Figure 7: Visualization of attention scores at different stages of layer attention on the ResNet-50 backbone for ImageNet-1K.